Available online at www.sciencedirect.com
ScienceDirect
Mechanics of Materials 39 (2007) 548–563
MECHANICS OF MATERIALS
www.elsevier.com/locate/mechmat

A stochastic micromechanical model for elastic properties of functionally graded materials

S. Rahman *, A. Chakraborty

Department of Mechanical and Industrial Engineering, The University of Iowa, 2140 Seamans Center, Iowa City, IA 52242, USA

Received 20 May 2006; received in revised form 19 August 2006

Abstract

A stochastic micromechanical model is presented for predicting probabilistic characteristics of elastic mechanical properties of an isotropic functionally graded material (FGM) subject to statistical uncertainties in material properties of constituents and their respective volume fractions. The model involves non-homogeneous, non-Gaussian random field representation of phase volume fractions and random variable description of constituent material properties, a three-phase Mori–Tanaka model for underlying micromechanics and homogenization, and a novel dimensional decomposition method for obtaining probabilistic descriptors of effective FGM properties. Four numerical examples involving statistical properties of input random fields, limited experimental validation, and the second-moment characteristics and probability density functions of effective mechanical properties of FGM illustrate the proposed stochastic model. The results indicate that the model provides both accurate and computationally efficient estimates of probabilistic characteristics of effective FGM properties.

Keywords: Stochastic micromechanics; Random field; Effective properties; Second-moment characteristics; Dimensional decomposition method; Monte Carlo simulation

1. Introduction

Functionally graded materials (FGMs) are two- or multi-phase particulate composites in which material composition and microstructure vary spatially in the macroscopic length scale to meet a desired functional performance. The absence of sharp interfaces in FGM reduces material property mismatch, which can lead to significant improvement in damage resistance and mechanical durability (Suresh and Mortensen, 1998). Therefore, FGMs are of great interest in disciplines as diverse as civil infrastructure, aerospace propulsion, microelectronics, biomechanics, nuclear power, and nanotechnology (Suresh, 2001). However, the extent to which an FGM can be tailored to produce a target mechanical performance – i.e., the design of FGM – strongly depends on the resultant effective properties and, more importantly, on how these properties relate to its microstructure. Therefore, predicting

* Corresponding author. Tel.: +319 335 5679; fax: +319 335 5669.
E-mail address: rahman@engineering.uiowa.edu (S. Rahman).
URL: http://www.engineering.uiowa.edu/~rahman (S. Rahman).

0167-6636/$ - see front matter © 2006 Elsevier Ltd. All rights reserved.
doi:10.1016/j.mechmat.2006.08.006

mechanical, thermal, or other relevant properties for a given microstructure and its spatial distribution plays a significant role in the design of FGM.

In classical micromechanics (Mura, 1991; Nemat-Nasser and Hori, 1999), a wide variety of models exists for predicting effective properties of heterogeneous materials, such as rules of mixture and their bounds (Mura, 1991; Nemat-Nasser and Hori, 1999), the Hashin–Shtrikman model (Hashin and Strikman, 1963), the Eshelby's equivalent inclusion theory (Eshelby, 1957), the self-consistent model (Hill, 1965), the mean-field theory (Weng, 1984), and the Mori–Tanaka model (Mori and Tanaka, 1973). For FGM applications, a higher-order thermoelastic theory was developed by coupling local and global effects (Aboudi et al., 1996). Recently, an elastic model including pair-wise particle interaction and gradient effects of phase volume fraction has also appeared (Yin et al., 2004). The determination of effective properties has also been demonstrated using the Voronoi cell finite element method (VCFEM) (Grujicic and Zhang, 1998). Although these predictive models are continuously evolving, they are strictly deterministic. In other words, microstructural features, such as phase volume fraction, shape and spatial arrangement of an included phase, and other relevant characteristics, must be defined locally with absolute certainty. This fundamental determinism of the classical micromechanics is a practical concern because there is sample-to-sample variability in FGM microstructural features (Ferrante and Graham-Brady, 2005). Furthermore, a viable FGM manufacturing technology to create a pre-determined microstructural profile can be produced only in a statistical sense. Using mean or median values of random microstructural details as input for predicting deterministic effective properties is not always meaningful, as it does not provide any measures of the stochastic behavior of FGM. As a few researchers have already pointed out, a predictive micromechanical model must include statistical variability of phase volume fractions as random input (Ferrante and Graham-Brady, 2005; Buryachenko and Rammerstorfer, 2001). Therefore, it makes sense to formulate and explore the FGM micromechanics problem in a stochastic framework.

This paper presents a stochastic micromechanical model for predicting probabilistic characteristics of elastic mechanical properties of an isotropic FGM subject to statistical uncertainties in volume fractions of particle and porosity and constituent material properties. The model involves (1) non-homogeneous, non-Gaussian random field representation of phase volume fractions and random variable description of constituent material properties; (2) a three-phase Mori–Tanaka model for underlying micromechanics and homogenization; and (3) novel dimensional decomposition methods for probabilistic descriptors of effective mechanical properties. Section 2 describes the problem of interest, random field and random variable models of various input parameters, and the three-phase Mori–Tanaka model. Section 3 explains the newly developed decomposition methods for predicting statistical moments and probability density functions of effective mechanical properties of FGM. Four examples involving statistical properties of input random fields, limited experimental validations, and stochastic characteristics of effective properties of FGM illustrate the proposed model in Section 4. Finally, Section 5 provides conclusions from this work.

2. Stochastic micromechanics

2.1. Problem definition

Consider a three-phase FGM heterogeneous body with domain $\mathscr{D} \subset \mathbb{R}^3$ and a schematic illustration of its microstructure, as shown in Fig. 1. The microstructure includes three distinct material phases: phase 1 (grey), phase 2 (black), and phase 3 (white), each of which represents an isotropic

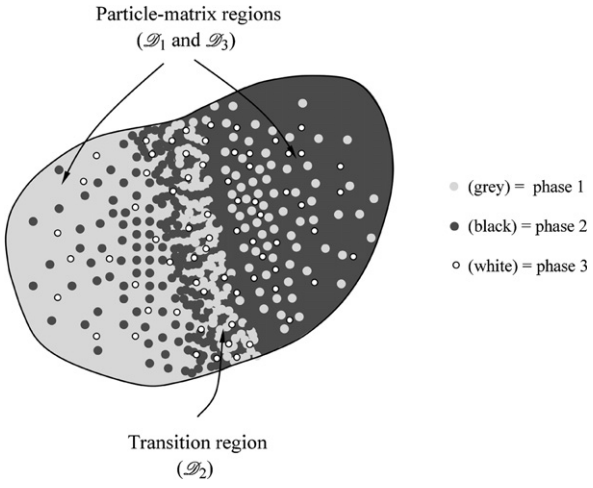

Fig. 1. Schematic representation of a three-phase FGM.

and linear-elastic material. The stochastic elasticity tensors of these three phases, denoted by $\boldsymbol{C}^{(1)}$, $\boldsymbol{C}^{(2)}$, and $\boldsymbol{C}^{(3)}$, can be expressed by (Mura, 1991; Nemat-Nasser and Hori, 1999)

$$\boldsymbol{C}^{(i)} = \frac{v_i E_i}{(1+v_i)(1-2v_i)}\mathbf{1}\otimes\mathbf{1} + \frac{E_i}{(1+v_i)}\boldsymbol{I}; \quad i = 1,2,3, \tag{1}$$

where the symbol $\otimes$ denotes tensor product; E_i and v_i are respectively elastic modulus and Poisson's ratio of phase i; and $\mathbf{1}$ and $\boldsymbol{I}$ are respectively second- and fourth-rank identity tensors. In general, E_i and v_i are random variables because of statistical variation in the material properties of each constituent phase. One phase defines the matrix material, and the remaining two characterize ellipsoidal particles. Two classes of particles allow modeling multi-phase FGM with distinct properties of its first (grey or black) and second (white) classes of inclusions. Material porosities, if they exist, can also be conveniently modeled as voids by employing degenerative properties of the second class of particles, leading to two-phase porous FGMs.

Fig. 2 illustrates three disjoint FGM regions in the macroscopic length scale ($\boldsymbol{x}$) with subdomains $\mathscr{D}_1$, $\mathscr{D}_2$, and $\mathscr{D}_3$, where $\mathscr{D} = \bigcup_{i=1}^{3}\mathscr{D}_i$; $\mathscr{D}_i \cap \mathscr{D}_j = \emptyset$, $i \neq j$. The particle–matrix region 1 ($\mathscr{D}_1$), depicted in Fig. 2(a), comprises particles from phase 2 material (black) embedded in the matrix material, which is phase 1 (grey). The particle–matrix role reverses in region 3 ($\mathscr{D}_3$), where particles and matrix are phase 1 (grey) and phase 2 (black) materials, respectively, as shown in Fig. 2(c). In the transition region 2 ($\mathscr{D}_2$), illustrated by Fig. 2(b), the definition of particle or matrix is ambiguous as both phases have interpenetrated each other, forming intertwined clusters. If there are porosities, phase 3 material (white) may exist as voids in each region with a distribution depending on the fabrication process.

Let $\boldsymbol{x} \in \mathscr{D} \subset \mathbb{R}^3$ define a point in the macroscopic length scale. The volume fractions of material phases 1, 2, and 3 are respectively denoted by $\phi_1(\boldsymbol{x})$, $\phi_2(\boldsymbol{x})$, and $\phi_3(\boldsymbol{x})$, each of which is bounded

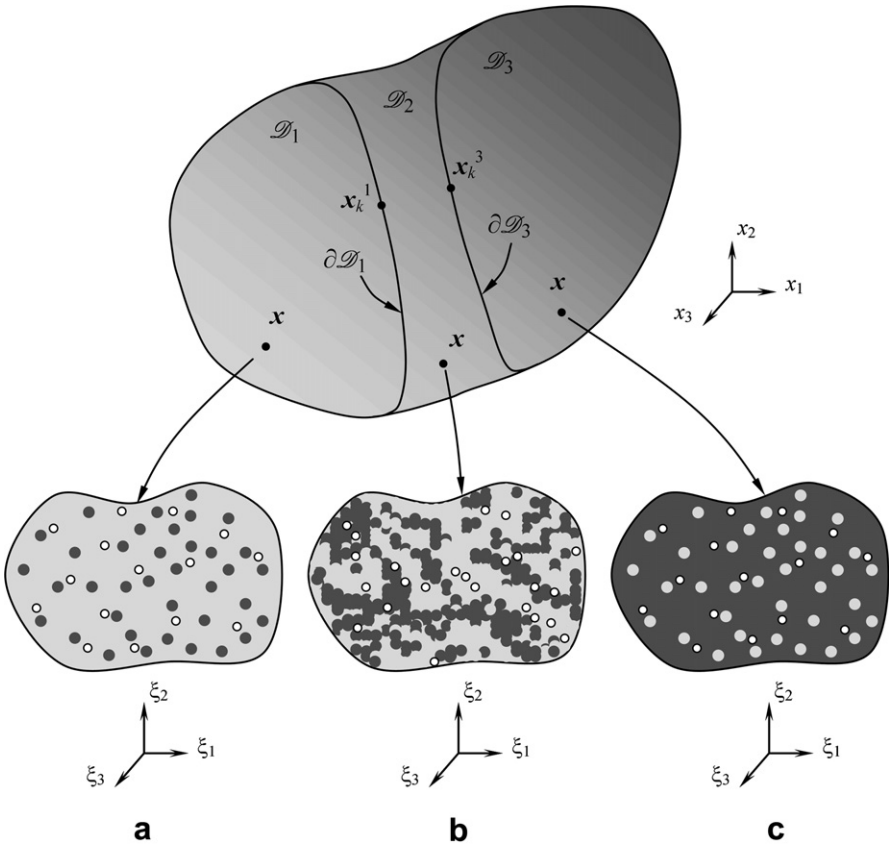

Fig. 2. Three macroscopic regions and associated RVEs in microscopic length scale (ξ); (a) particle–matrix region 1; (b) transition region 2 and (c) particle–matrix region 3.

between 0 and 1 and satisfy the constraint $\phi_1(\boldsymbol{x}) + \phi_2(\boldsymbol{x}) + \phi_3(\boldsymbol{x}) = 1$. The volume fractions are stochastic and must be modeled as random fields due to their spatial variability. A representative volume element (RVE) at $\boldsymbol{x}$ characterizes material heterogeneity in the microscopic length scale with the coordinate system $\boldsymbol{\xi} \equiv (\xi_1, \xi_2, \xi_3)$. Since the FGM microstructure varies in the macroscopic length scale, two distinct points in Fig. 2 will have two distinct RVEs. For an RVE associated with $\boldsymbol{x} \in \mathscr{D}_1 \cup \mathscr{D}_3$, volume fractions of the matrix, the first class of particles, and the second class of particles, respectively denoted by $\phi_m(\boldsymbol{x})$, $\phi_p(\boldsymbol{x})$, and $\phi_v(\boldsymbol{x})$, are related to volume fractions of constituent materials as

$$\phi_m(\boldsymbol{x}) = \begin{cases} \phi_1(\boldsymbol{x}), & \text{if } \boldsymbol{x} \in \mathscr{D}_1, \\ \phi_2(\boldsymbol{x}), & \text{if } \boldsymbol{x} \in \mathscr{D}_3, \end{cases} \tag{2}$$

$$\phi_p(\boldsymbol{x}) = \begin{cases} \phi_2(\boldsymbol{x}), & \text{if } \boldsymbol{x} \in \mathscr{D}_1, \\ \phi_1(\boldsymbol{x}), & \text{if } \boldsymbol{x} \in \mathscr{D}_3, \end{cases} \tag{3}$$

and

$$\phi_v(\boldsymbol{x}) = \phi_3(\boldsymbol{x}) = 1 - \phi_m(\boldsymbol{x}) - \phi_p(\boldsymbol{x}), \quad \text{if } \boldsymbol{x} \in \mathscr{D}_1 \cup \mathscr{D}_3. \tag{4}$$

A major objective of stochastic micromechanics is to obtain probabilistic characteristics of effective properties when random elastic properties of its constituents (e.g., E_i and ν_i) and random volume fractions of any two material phases (e.g., $\phi_2(\boldsymbol{x})$ and $\phi_3(\boldsymbol{x})$) are prescribed.

2.2. Stochastic description of volume fractions by random fields

Let $(\Omega, \mathscr{F}, P)$ be a probability space, where Ω is the sample space, $\mathscr{F}$ is the σ-algebra of subsets of Ω, and P is the probability measure, and $\mathbb{R}^N$ be an N-dimensional real vector space. Defined on the probability triple $(\Omega, \mathscr{F}, P)$ endowed with the expectation operator $\mathbb{E}$, consider a non-homogeneous (non-stationary), non-Gaussian, random field $\phi_i(\boldsymbol{x})$; $i = 1, 2, 3$, which has mean $\mu_i(\boldsymbol{x})$ and standard deviation $\sigma_i(\boldsymbol{x})$. The standardized phase volume fraction

$$\tilde{\phi}_i(\boldsymbol{x}) = \frac{\phi_i(\boldsymbol{x}) - \mu_i(\boldsymbol{x})}{\sigma_i(\boldsymbol{x})}, \tag{5}$$

which has zero mean and unit variance, is at least a weakly homogeneous (stationary) random field with prescribed covariance function $\Gamma_{\tilde{\phi}_i}(\boldsymbol{s}) \equiv \mathbb{E}[\tilde{\phi}_i(\boldsymbol{x})\tilde{\phi}_i(\boldsymbol{x}+\boldsymbol{s})]$ and marginal cumulative distribution function $F_i(\tilde{\phi}_i)$ such that $0 \leqslant \phi_i(\boldsymbol{x}) \leqslant 1$ with probability one.

2.2.1. Translation random field

Consider a zero-mean, homogeneous, Gaussian random field $\alpha_i(\boldsymbol{x})$ with the covariance function $\Gamma_{\alpha_i}(\boldsymbol{s}) \equiv \mathbb{E}[\alpha_i(\boldsymbol{x})\alpha_i(\boldsymbol{x}+\boldsymbol{s})]$, which is continuous over $\mathscr{D}$. If G_i is a real-valued, monotonic, differentiable function, the standardized phase volume fraction

$$\tilde{\phi}_i(\boldsymbol{x}) = G_i[\alpha_i(\boldsymbol{x})] \tag{6}$$

can be viewed as a memoryless transformation of the Gaussian image field $\alpha_i(\boldsymbol{x})$. From the condition that the marginal distribution and the covariance function of $\tilde{\phi}_i(\boldsymbol{x})$ coincide with specified target functions F_i and $\Gamma_{\tilde{\phi}_i}$, respectively, it can be shown that (Grigoriu, 1995)

$$G_i(\alpha_i) = F_i^{-1}[\Phi(\alpha_i)] \tag{7}$$

and

$$\Gamma_{\tilde{\phi}_i}(\boldsymbol{s}) = \int_{-\infty}^{\infty}\int_{-\infty}^{\infty} G_i(\eta_1)G_i(\eta_2)\varphi_2(\eta_1, \eta_2, \Gamma_{\alpha_i}(\boldsymbol{s}))\,\mathrm{d}\eta_1\,\mathrm{d}\eta_2, \tag{8}$$

where $\Phi(\alpha_i) \equiv \int_{-\infty}^{\alpha_i}(1/\sqrt{2\pi})\exp(-\eta^2/2)\,\mathrm{d}\eta$ is the standard Gaussian distribution function and $\varphi_2(\eta_1, \eta_2, \Gamma_{\alpha_i})$ is the bivariate standard Gaussian density function with the correlation coefficient Γ_{α_i}. For given values of F_i and $\Gamma_{\tilde{\phi}_i}(\boldsymbol{s})$, G_i can be calculated from Eq. (7) and the required covariance function $\Gamma_{\alpha_i}(\boldsymbol{s})$ of $\alpha_i(\boldsymbol{x})$ can be solved from Eq. (8), if the target scaled covariance function $\Gamma_{\tilde{\phi}_i}(\boldsymbol{s})/\Gamma_{\tilde{\phi}_i}(\boldsymbol{0})$ lie in the range (Grigoriu, 1995)

$$\frac{\mathbb{E}[G_i(\alpha_i)G_i(-\alpha_i)] - \mathbb{E}[G_i(\alpha_i)]^2}{\mathbb{E}[G_i(\alpha_i)^2] - \mathbb{E}[G_i(\alpha_i)]^2} \leqslant \frac{\Gamma_{\tilde{\phi}_i}(\boldsymbol{s})}{\Gamma_{\tilde{\phi}_i}(\boldsymbol{0})} \leqslant 1. \tag{9}$$

In many applications, Inequality (9) is satisfied, leading to the standardized volume fraction $\tilde{\phi}_i(\boldsymbol{x})$ that can be mapped to the associated Gaussian image field $\alpha_i(\boldsymbol{x})$.

2.2.2. Karhunen–Loève approximation

Let $\{\lambda_{i,k}, \psi_{i,k}(\boldsymbol{x})\}$, $k = 1, 2, \ldots, \infty$, be the eigenvalues and eigenfunctions of $\Gamma_{\alpha_i}(\boldsymbol{s}) \equiv \mathbb{E}[\alpha_i(\boldsymbol{x})\alpha_i(\boldsymbol{x}+\boldsymbol{s})] \equiv \Gamma_i(\boldsymbol{x}_1, \boldsymbol{x}_2)$; $\boldsymbol{x}_1 = \boldsymbol{x}$, $\boldsymbol{x}_2 = \boldsymbol{x} + \boldsymbol{s}$ that satisfy the integral equation (Davenport and Root, 1958)

$$\int_{\mathscr{D}} \Gamma_i(\boldsymbol{x}_1, \boldsymbol{x}_2)\psi_{i,k}(\boldsymbol{x}_2)\,\mathrm{d}\boldsymbol{x}_2 = \lambda_{i,k}\psi_{i,k}(\boldsymbol{x}_1), \quad \forall k = 1, 2, \ldots, \infty. \tag{10}$$

The eigenfunctions are orthogonal in the sense that

$$\int_{\mathscr{D}} \psi_{i,k}(\boldsymbol{x})\psi_{i,l}(\boldsymbol{x})\,\mathrm{d}\boldsymbol{x} = \delta_{kl}, \quad \forall k, l = 1, 2, \ldots, \infty, \tag{11}$$

where δ_{kl} is the Kronecker delta. The Karhunen–Loève (K–L) representation of $\alpha_i(\boldsymbol{x})$ is

$$\alpha_i(\boldsymbol{x}) = \sum_{k=1}^{\infty} Z_{i,k}\sqrt{\lambda_{i,k}}\psi_{i,k}(\boldsymbol{x}), \tag{12}$$

where $Z_{i,k}$, $k = 1, \ldots, \infty$ is an infinite sequence of uncorrelated Gaussian random variables, each of which has *zero* mean and *unit* variance. In practice, the infinite series of Eq. (12) must be truncated, yielding a K–L approximation

$$\hat{\alpha}_i(\boldsymbol{x}) = \sum_{k=1}^{M} Z_{i,k}\sqrt{\lambda_{i,k}}\psi_{i,k}(\boldsymbol{x}), \tag{13}$$

which approaches $\alpha_i(\boldsymbol{x})$ in the mean square sense as the positive integer $M \to \infty$. Finite element (Ghanem and Spanos, 1991) or mesh-free (Rahman and Xu, 2005) methods can be readily applied to obtain eigensolutions of any covariance function and domain of the random field. For linear or exponential covariance functions and simple domains, the eigensolutions can be evaluated analytically (Ghanem and Spanos, 1991).

Once $\Gamma_{\alpha_i}(\boldsymbol{s})$ and its eigensolutions are determined, the parameterization of $\tilde{\phi}_i(\boldsymbol{x})$ is achieved by the K–L approximation of its Gaussian image, i.e.,

$$\tilde{\phi}_i(\boldsymbol{x}) \cong G_i\left[\sum_{k=1}^{M} Z_{i,k}\sqrt{\lambda_{i,k}}\psi_{i,k}(\boldsymbol{x})\right]. \tag{14}$$

According to Eq. (14), the K–L approximation provides a parametric representation of the standardized volume fraction $\tilde{\phi}_i(\boldsymbol{x})$ and, hence, of $\phi_i(\boldsymbol{x})$ with M random variables. The random field description of $\phi_i(\boldsymbol{x})$ allows a volume fraction to have random fluctuation at a point $\boldsymbol{x}$ in the macroscopic length scale.

2.3. Stochastic description of constituent material properties by random variables

In addition to spatially variant random volume fractions, the constituent properties of material phases can be stochastic. Defined on the same probability space $(\Omega, \mathscr{F}, P)$, let E_i and v_i denote the elastic modulus and Poisson's ratio, respectively, of the ith material phase. Therefore, the random vector $\{E_1, E_2, E_3, v_1, v_2, v_3\}^{\mathrm{T}} \in \mathbb{R}^6$ describes stochastic elastic properties of all three constituents. Unlike volume fractions, however, the constituent properties are spatially invariant in the macroscopic ($\boldsymbol{x}$) length scale. In addition, for a given $\boldsymbol{x} \in \mathscr{D}$, the volume fractions and constituent properties, although both stochastic, do not vary spatially in the microscopic (ξ) length scale. The probability density function of constituent material properties is either assumed or derived from available material characterization data.

If N is the total number of possible random variables including $2M$ random variables due to the discretization of random fields $\tilde{\phi}_2(\boldsymbol{x})$ and $\tilde{\phi}_3(\boldsymbol{x})$ and six random constituent properties, the maximum value of N is $2M + 6$. Hence, an input random vector $\boldsymbol{R} = \{Z_{2,1}, \ldots, Z_{2,M}, Z_{3,1}, \ldots, Z_{3,M}, E_1, E_2, E_3, v_1, v_2, v_3\}^{\mathrm{T}} \in \mathbb{R}^N$ characterizes uncertainties from all sources in an FGM and is completely described by its known joint probability density function $f_{\boldsymbol{R}}(\boldsymbol{r}) : \mathbb{R}^N \mapsto \mathbb{R}$.

2.4. Effective properties at particle–matrix regions

Consider a single, linear-elastic, isotropic, ellipsoidal particle of domain Ω_p and elasticity tensor $\boldsymbol{C}^{(p)}$, which is embedded in an infinitely large linear-elastic isotropic matrix of domain Ω_m and elasticity tensor $\boldsymbol{C}^{(m)}$, as shown in Fig. 3(a). The single particle–matrix system, which has a local coordinate system $\boldsymbol{\xi} \equiv (\xi_1, \xi_2, \xi_3)$, is subjected to a uniform far-field stress $\boldsymbol{\sigma}_0$. Let $\boldsymbol{\varepsilon}(\boldsymbol{\xi})$ and $\boldsymbol{\sigma}(\boldsymbol{\xi})$ define local elastic strain and stress fields, respectively, inside the particle ($\boldsymbol{\xi} \in \Omega_p$). Using the Eshelby's equivalent inclusion method (Eshelby, 1957), the decomposition of the elasticity problem depicted in Fig. 3(a) for an infinite domain yields

$$\boldsymbol{\varepsilon}(\boldsymbol{\xi}) = \boldsymbol{\varepsilon}_0 + \boldsymbol{S} : \boldsymbol{\varepsilon}^*; \quad \boldsymbol{\xi} \in \Omega_p, \tag{15}$$

$$\boldsymbol{\sigma}(\boldsymbol{\xi}) = \boldsymbol{\sigma}_0 + \boldsymbol{C}^{(m)} \cdot [\boldsymbol{S} - \boldsymbol{I}] : \boldsymbol{\varepsilon}^*; \quad \boldsymbol{\xi} \in \Omega_p, \tag{16}$$

where symbols "$\cdot$" and ":" denote tensor contractions between two fourth-rank tensors and between fourth- and second-rank tensors, respectively, $\boldsymbol{\varepsilon}_0 = [\boldsymbol{C}^{(m)}]^{-1} : \boldsymbol{\sigma}_0$, eigenstrain $\boldsymbol{\varepsilon}^* = [(\boldsymbol{C}^{(p)} - \boldsymbol{C}^{(m)}) \cdot \boldsymbol{S} + \boldsymbol{C}^{(m)}]^{-1} \cdot (\boldsymbol{C}^{(m)} - \boldsymbol{C}^{(p)}) \cdot [\boldsymbol{C}^{(p)}]^{-1} : \boldsymbol{\sigma}_0$, $\boldsymbol{T}(\boldsymbol{\xi}, \boldsymbol{\eta})$ is the fourth-rank Green's function tensor that depends on the shear modulus and Poisson's ratio of the matrix material, and $\boldsymbol{S} = \int_{\Omega_p} \boldsymbol{T}(\boldsymbol{\xi}, \boldsymbol{\eta})\,\mathrm{d}\boldsymbol{\eta}$ is the fourth-rank Eshelby's interior-point tensor. For an ellipsoidal domain, $\boldsymbol{S}$ is independent of $\boldsymbol{\xi} \in \Omega_p$, leading to constant stress and strain inside the particle.

For the FGM, consider an RVE at $\boldsymbol{x} \in \mathscr{D}_1 \cup \mathscr{D}_3$, where an infinite number of ellipsoidal particles from both classes, each with respective total

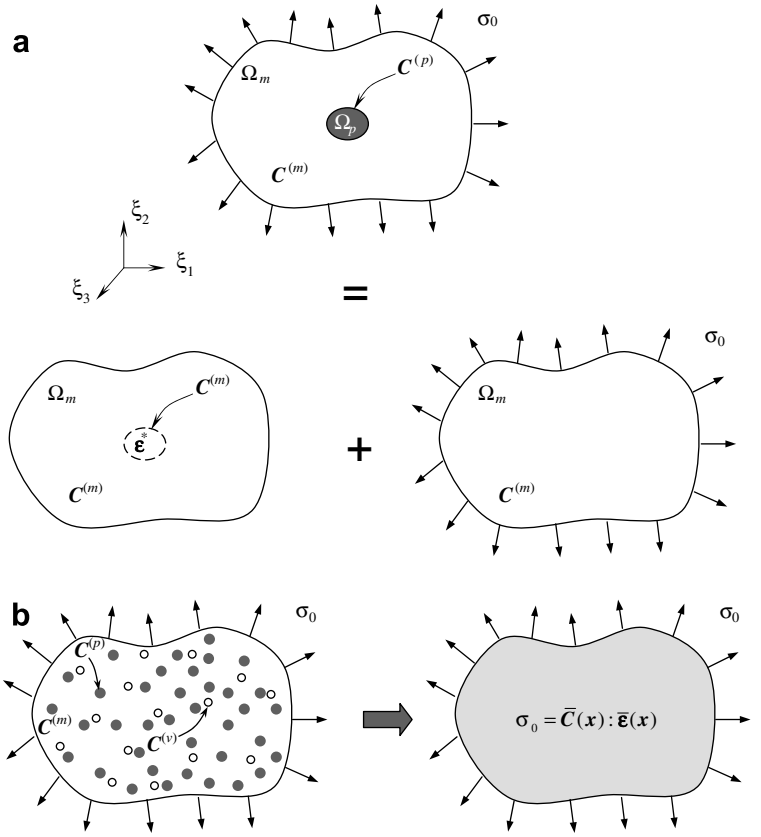

Fig. 3. Micromechanics: (a) Eshelby's equivalent inclusion; (b) homogenization.

domains $\Omega_p(\boldsymbol{x})$ and $\Omega_v(\boldsymbol{x})$ and respective elasticity tensors $\boldsymbol{C}^{(p)}$ and $\boldsymbol{C}^{(v)}$, are filled in a matrix of domain $\Omega_m(\boldsymbol{x})$ and elasticity tensor $\boldsymbol{C}^{(m)}$, as shown in Fig. 3(b). Since phase volume fractions of a given RVE depend on $\boldsymbol{x}$, the matrix and total particle domains with their volumes $V_m(\boldsymbol{x})$, $V_p(\boldsymbol{x})$, and $V_v(\boldsymbol{x})$ are spatially variant. So are the volume-averaged strains at the matrix, the first class of particles, and the second class of particles, which are defined as $\bar{\boldsymbol{\varepsilon}}_m(\boldsymbol{x}) \equiv [1/V_m(\boldsymbol{x})]\int_{V_m(\boldsymbol{x})}\boldsymbol{\varepsilon}(\boldsymbol{\xi})\,\mathrm{d}\boldsymbol{\xi}$, $\bar{\boldsymbol{\varepsilon}}_p(\boldsymbol{x}) \equiv [1/V_p(\boldsymbol{x})]\int_{V_p(\boldsymbol{x})}\boldsymbol{\varepsilon}(\boldsymbol{\xi})\,\mathrm{d}\boldsymbol{\xi}$, and $\boldsymbol{\varepsilon}_v(\boldsymbol{x}) \equiv [1/V_v(\boldsymbol{x})]\times\int_{V_v(\boldsymbol{x})}\boldsymbol{\varepsilon}(\boldsymbol{\xi})\,\mathrm{d}\boldsymbol{\xi}$, respectively. Using the equilibrium equation, these average strains can be related to the far-field uniform stress

$$\boldsymbol{\sigma}_0 = \phi_p(\boldsymbol{x})\boldsymbol{C}^{(p)} : \bar{\boldsymbol{\varepsilon}}_p(\boldsymbol{x}) + \phi_v(\boldsymbol{x})\boldsymbol{C}^{(v)} : \bar{\boldsymbol{\varepsilon}}_v(\boldsymbol{x}) + [1-\phi_p(\boldsymbol{x})-\phi_v(\boldsymbol{x})]\boldsymbol{C}^{(m)} : \bar{\boldsymbol{\varepsilon}}_m(\boldsymbol{x}); \quad \boldsymbol{x}\in\mathscr{D}_1\cup\mathscr{D}_3. \tag{17}$$

By applying the Mori–Tanaka model, which involves Eshelby's equivalent-inclusion solution for infinite number of particles and the assumption that an additional particle does not significantly change volume fractions, the relationship between average particle strain and average matrix strain can be obtained as (Mori and Tanaka, 1973)

$$\bar{\boldsymbol{\varepsilon}}_p(\boldsymbol{x}) = [\boldsymbol{I}-\boldsymbol{S}\cdot[\boldsymbol{C}^{(m)}]^{-1}\cdot(\boldsymbol{C}^{(p)}-\boldsymbol{C}^{(m)})]^{-1} : \bar{\boldsymbol{\varepsilon}}_m(\boldsymbol{x}); \quad \boldsymbol{x}\in\mathscr{D}_1\cup\mathscr{D}_3, \tag{18}$$

$$\bar{\boldsymbol{\varepsilon}}_v(\boldsymbol{x}) = [\boldsymbol{I}-\boldsymbol{S}\cdot[\boldsymbol{C}^{(m)}]^{-1}\cdot(\boldsymbol{C}^{(v)}-\boldsymbol{C}^{(m)})]^{-1} : \bar{\boldsymbol{\varepsilon}}_m(\boldsymbol{x}); \quad \boldsymbol{x}\in\mathscr{D}_1\cup\mathscr{D}_3. \tag{19}$$

Using Eqs. (17)–(19), three unknown volume-averaged strains $\bar{\boldsymbol{\varepsilon}}_m(\boldsymbol{x})$, $\bar{\boldsymbol{\varepsilon}}_p(\boldsymbol{x})$, and $\bar{\boldsymbol{\varepsilon}}_v(\boldsymbol{x})$ can be calculated at any macroscopic point $\boldsymbol{x}\in\mathscr{D}_1\cup\mathscr{D}_3$ for known values of applied stress, volume fractions and elasticity tensors of material phases, and Eshelby's interior-point tensor.

Let $\overline{\boldsymbol{C}}(\boldsymbol{x})$ denote the effective elasticity tensor at a point $\boldsymbol{x}\in\mathscr{D}_1\cup\mathscr{D}_3$. Based on the equilibrium equation,

$$\boldsymbol{\sigma}_0 = \overline{\boldsymbol{C}}(\boldsymbol{x}) : \bar{\boldsymbol{\varepsilon}}(\boldsymbol{x}); \quad \boldsymbol{x}\in\mathscr{D}_1\cup\mathscr{D}_3, \tag{20}$$

where

$$\bar{\boldsymbol{\varepsilon}}(\boldsymbol{x}) \equiv \phi_p(\boldsymbol{x})\bar{\boldsymbol{\varepsilon}}_p(\boldsymbol{x}) + \phi_v(\boldsymbol{x})\bar{\boldsymbol{\varepsilon}}_v(\boldsymbol{x}) + [1-\phi_p(\boldsymbol{x})-\phi_v(\boldsymbol{x})]\bar{\boldsymbol{\varepsilon}}_m(\boldsymbol{x}); \quad \boldsymbol{x}\in\mathscr{D}_1\cup\mathscr{D}_3 \tag{21}$$

is the volume-averaged strain in the homogenized RVE that can be calculated following the solution of Eqs. (17)–(19) for $\bar{\boldsymbol{\varepsilon}}_m(\boldsymbol{x})$, $\bar{\boldsymbol{\varepsilon}}_p(\boldsymbol{x})$, and $\bar{\boldsymbol{\varepsilon}}_v(\boldsymbol{x})$. Therefore, the effective tensor $\overline{\boldsymbol{C}}(\boldsymbol{x})$ can be evaluated from Eq. (20) when $\boldsymbol{\sigma}_0$ and $\bar{\boldsymbol{\varepsilon}}(\boldsymbol{x})$ are known. Defining

$$\overline{\boldsymbol{C}}(\boldsymbol{x}) = \frac{\bar{\nu}(\boldsymbol{x})\overline{E}(\boldsymbol{x})}{[1+\bar{\nu}(\boldsymbol{x})][1-2\bar{\nu}(\boldsymbol{x})]}\mathbf{1}\otimes\mathbf{1} + \frac{\overline{E}(\boldsymbol{x})}{[1+\bar{\nu}(\boldsymbol{x})]}\boldsymbol{I} \tag{22}$$

the effective elastic modulus $\overline{E}(\boldsymbol{x})$ and effective Poisson's ratio $\bar{\nu}(\boldsymbol{x})$ can thus be evaluated at any macroscopic point $\boldsymbol{x} \in \mathscr{D}_1 \cup \mathscr{D}_3$.

2.5. Effective properties at transition region

The particle and matrix are well-defined when a phase volume fraction is close to 0 or 1. However, when a volume fraction is in the vicinity of 0.5, it is difficult to identify the particle or the matrix phase, as in the transition region 2. Consequently, the homogenized elastic fields for a transition region cannot be determined from a classical micromechanical analysis. However, in a realistic FGM, the transition region $\mathscr{D}_2$, which lies between boundaries $\partial\mathscr{D}_1$ and $\partial\mathscr{D}_3$ as shown in Fig. 2, is much smaller than the particle–matrix regions 1 and 3. In that case, the effective properties at the transition region can be approximated using interpolation of the micromechanical results of particle–matrix regions.

In the macroscopic scale, consider collections of K points $\{\boldsymbol{x}_k^1 \in \partial\mathscr{D}_1;\ k = 1,\ldots K\}$ and $\{\boldsymbol{x}_k^3 \in \partial\mathscr{D}_3;\ k = 1,\ldots K\}$ located at boundaries $\partial\mathscr{D}_1$ and $\partial\mathscr{D}_3$, respectively. Let $\{\bar{\boldsymbol{\varepsilon}}^1(\boldsymbol{x}_k^1);\ k = 1,\ldots K\}$ and $\{\bar{\boldsymbol{\varepsilon}}^3(\boldsymbol{x}_k^3);\ k = 1,\ldots K\}$ represent volume-averaged strains of homogenized RVEs at $\{\boldsymbol{x}_k^1 \in \partial\mathscr{D}_1;\ \ k = 1,\ldots K\}$ and $\{\boldsymbol{x}_k^3 \in \partial\mathscr{D}_3;\ k = 1,\ldots K\}$, respectively, which can be determined from particle–matrix equations (e.g., Eqs. (17)–(19) and (21)). The interpolated volume-averaged strain of a homogenized RVE at the transition zone depends on volume-averaged strains at boundaries $\partial\mathscr{D}_1$ and $\partial\mathscr{D}_3$ and a judiciously chosen interpolation function $w(\boldsymbol{x})$. The interpolation function can be derived by forcing continuity, differentiability, and other relevant properties of average strains. Implicitly,

$$\bar{\boldsymbol{\varepsilon}}(\boldsymbol{x}) = f\big(\bar{\boldsymbol{\varepsilon}}^1(\boldsymbol{x}_1^1),\ldots,\bar{\boldsymbol{\varepsilon}}^1(\boldsymbol{x}_K^1);\ \bar{\boldsymbol{\varepsilon}}^3(\boldsymbol{x}_1^3),\ldots,\bar{\boldsymbol{\varepsilon}}^3(\boldsymbol{x}_K^3); w(\boldsymbol{x})\big);\quad \boldsymbol{x} \in \mathscr{D}_2, \tag{23}$$

which, when combined with Eqs. (20) and (22), yields effective elastic properties at a macroscopic point $\boldsymbol{x} \in \mathscr{D}_2$ in the transition region. Explicit forms of f and $w(\boldsymbol{x})$ depend on the FGM geometry and gradation properties.

Eqs. (15)–(23) provide a deterministic micromechanics framework for predicting effective properties of FGM. However, any statistical uncertainties in volume fractions and constituent material properties, represented by a random vector $\boldsymbol{R}$, must be propagated through these micromechanical equations. Therefore, an effective FGM property is not only spatially variant, but also randomly dependent on $\boldsymbol{R}$, and should be expressed as a function of both $\boldsymbol{x}$ and $\boldsymbol{R}$. Henceforth, let $y(\boldsymbol{R};\boldsymbol{x})$ describe a generic, but relevant elastic property (e.g., the effective elastic modulus or the effective Poisson's ratio) at $\boldsymbol{x} \in \mathscr{D}$ for a given FGM problem of interest. In general, for a given spatial location ($\boldsymbol{x}$), the multivariate function $y(\boldsymbol{r};\boldsymbol{x})$ is implicit and can only be viewed as a high-dimensional input–output mapping, where the evaluation of the output function y for a given input $\boldsymbol{r}$ requires classical micromechanical analysis. Therefore, methods employed in stochastic micromechanics must be capable of generating accurate probabilistic characteristics of $y(\boldsymbol{R};\boldsymbol{x})$ with an acceptably small number of output function evaluations.

3. Dimensional decomposition method

At a given $\boldsymbol{x} \in \mathscr{D}$, consider a continuous, differentiable, real-valued function $y(\boldsymbol{r};\boldsymbol{x})$ that depends on $\boldsymbol{r} = \{r_1,\ldots,r_N\}^{\mathrm{T}} \in \mathbb{R}^N$. A dimensional decomposition of $y(\boldsymbol{r};\boldsymbol{x})$, described by Xu and Rahman (2004, 2005)

$$y(\boldsymbol{r};\boldsymbol{x}) = \underbrace{\underbrace{\underbrace{y_0(\boldsymbol{x}) + \sum_{i=1}^{N} y_i(r_i;\boldsymbol{x})}_{=\hat{y}_1(\boldsymbol{r};\boldsymbol{x})} + \sum_{\substack{i_1,i_2=1\\ i_1<i_2}}^{N} y_{i_1 i_2}(r_{i_1},r_{i_2};\boldsymbol{x})}_{=\hat{y}_2(\boldsymbol{r};\boldsymbol{x})} + \cdots + \sum_{\substack{i_1,\ldots,i_S=1\\ i_1<\cdots<i_S}}^{N} y_{i_1\cdots i_S}(r_{i_1},\ldots,r_{i_s};\boldsymbol{x})}_{=\hat{y}_S(\boldsymbol{r};\boldsymbol{x})} + \cdots + y_{12\ldots N}(r_1,\ldots,r_N;\boldsymbol{x}), \tag{24}$$

can be viewed as a finite hierarchical expansion of an output function in terms of its input variables with increasing dimensions, where $y_0(\boldsymbol{x})$ is a constant with respect to $\boldsymbol{r}$, $y_i(r_i;\boldsymbol{x})$ is a univariate component function representing individual contribution to $y(\boldsymbol{r};\boldsymbol{x})$ by input variable r_i acting alone, $y_{i_1 i_2}(r_{i_1}, r_{i_2};\boldsymbol{x})$ is a bivariate component function describing cooperative influence of two input variables r_{i_1} and r_{i_2}, $y_{i_1 \ldots i_S}(r_{i_1}, \ldots, r_{i_S};\boldsymbol{x})$ is an S-variate component function quantifying cooperative effects of S input variables $r_{i_1}, \ldots, r_{i_S}$, and so on. If

$$\hat{y}_S(\boldsymbol{r};\boldsymbol{x}) = y_0(\boldsymbol{x}) + \sum_{i=1}^{N} y_i(r_i;\boldsymbol{x}) + \sum_{\substack{i_1,i_2=1 \\ i_1<i_2}}^{N} y_{i_1 i_2}(r_{i_1}, r_{i_2};\boldsymbol{x}) + \cdots + \sum_{\substack{i_1,\ldots,i_S=1 \\ i_1<\cdots<i_S}}^{N} y_{i_1 \ldots i_S}(r_{i_1}, \ldots, r_{i_s};\boldsymbol{x}) \tag{25}$$

represents a general S-variate approximation of $y(\boldsymbol{r};\boldsymbol{x})$, the univariate ($S=1$) and bivariate ($S=2$) approximations $\hat{y}_1(\boldsymbol{r};\boldsymbol{x})$ and $\hat{y}_2(\boldsymbol{r};\boldsymbol{x})$ respectively provide two- and three-term approximants of the finite decomposition in Eq. (24). Similarly, trivariate, quadrivariate, and other higher-variate approximations can be derived by appropriately selecting the value of S. In the limit, when $S=N$, $\hat{y}_S(\boldsymbol{r};\boldsymbol{x})$ converges to the exact function $y(\boldsymbol{r};\boldsymbol{x})$. In other words, Eq. (25) generates a hierarchical and convergent sequence of approximations of $y(\boldsymbol{r};\boldsymbol{x})$.

3.1. Lower-variate approximations

Consider univariate and bivariate approximations of $y(\boldsymbol{r};\boldsymbol{x})$, defined by

$$\hat{y}_1(\boldsymbol{r};\boldsymbol{x}) \equiv \hat{y}_1(r_1, \ldots, r_N;\boldsymbol{x}) \equiv \sum_{i=1}^{N} \underbrace{y(c_1, \ldots, c_{i-1}, r_i, c_{i+1}, \ldots, c_N;\boldsymbol{x})}_{=y_i(r_i;\boldsymbol{x})} \underbrace{-(N-1)y(\boldsymbol{c};\boldsymbol{x})}_{=y_0(\boldsymbol{x})} \tag{26}$$

and

$$\hat{y}_2(\boldsymbol{r};\boldsymbol{x}) \equiv \hat{y}_2(r_1, \ldots, r_N;\boldsymbol{x}) \equiv \sum_{\substack{i_1,i_2=1 \\ i_1<i_2}}^{N} \overbrace{y(c_1, \ldots, c_{i_1-1}, r_{i_1}, c_{i_1+1}, \ldots, c_{i_2-1}, r_{i_2}, c_{i_2+1}, \ldots, c_N;\boldsymbol{x})}^{=y_{i_1 i_2}(r_{i_1}, r_{i_2};\boldsymbol{x})} + \sum_{i=1}^{N} \underbrace{-(N-2)y(c_1, \ldots, c_{i-1}, r_i, c_{i+1}, \ldots, c_N;\boldsymbol{x})}_{=y_i(r_i;\boldsymbol{x})} + \underbrace{\frac{(N-1)(N-2)}{2} y(\boldsymbol{c};\boldsymbol{x})}_{=y_0(\boldsymbol{x})}, \tag{27}$$

respectively, where $\boldsymbol{c} = \{c_1, \ldots, c_N\}^{\mathrm{T}}$ is a reference point in the input domain of $\boldsymbol{R}$, $y(\boldsymbol{c};\boldsymbol{x}) \equiv y(c_1, \ldots, c_N;\boldsymbol{x})$, $y_i(r_i;\boldsymbol{x}) \equiv y(c_1, \ldots, c_{i-1}, r_i, c_{i+1}, \ldots, c_N;\boldsymbol{x})$ and $y_{i_1 i_2}(r_{i_1}, r_{i_2};\boldsymbol{x}) \equiv y(c_1, \ldots, c_{i_1-1}, r_{i_1}, c_{i_1+1}, \ldots, c_{i_2-1}, r_{i_2}, c_{i_2+1}, \ldots, c_N;\boldsymbol{x})$. Based on the authors' past experience, the mean point of random input defines a suitable reference point. These univariate or bivariate approximations should not be viewed as first- or second-order Taylor series expansions nor do they limit the nonlinearity of $y(\boldsymbol{r};\boldsymbol{x})$. In fact, all higher-order univariate or bivariate terms of $y(\boldsymbol{r};\boldsymbol{x})$ are included in Eqs. (26) or (27), which should therefore generally provide a higher-order approximation of a multivariate function than equations derived from first- or second-order Taylor expansions.

3.2. Lagrange interpolations

Consider the univariate component function $y_i(r_i;\boldsymbol{x}) \equiv y(c_1, \ldots, c_{i-1}, r_i, c_{i+1}, \ldots, c_N;\boldsymbol{x})$ in Eq. (26) or (27). If for sample points $r_i = r_i^{(j)}$; $j = 1, \ldots, n$ of $\boldsymbol{R}$, n distinct function values $y(c_1, \ldots, c_{i-1}, r_i^{(j)}, c_{i+1}, \ldots, c_N;\boldsymbol{x})$; $j = 1, \ldots, n$ are given, the function value for an arbitrary r_i can be obtained by the Lagrange interpolation

$$y_i(r_i;\boldsymbol{x}) = \sum_{j=1}^{n} \zeta_j(r_i) y(c_1, \ldots, c_{i-1}, r_i^{(j)}, c_{i+1}, \ldots, c_N;\boldsymbol{x}), \tag{28}$$

where $\zeta_j(r_i) \equiv \prod_{k=1,k\neq j}^{n}(r_i - r_i^{(k)}) / \prod_{k=1,k\neq j}^{n}(r_i^{(j)} - r_i^{(k)})$ is the Lagrange shape function. The same idea can be applied to approximate the bivariate component function

$$y_{i_1 i_2}(r_{i_1}, r_{i_2};\boldsymbol{x}) = \sum_{j_2=1}^{n} \sum_{j_1=1}^{n} \zeta_{j_1}(r_{i_1}) \zeta_{j_2}(r_{i_2}) y(c_1, \ldots, c_{i_1-1}, r_{i_1}^{(j_1)}, c_{i_1+1}, \ldots, c_{i_2-1}, r_{i_2}^{(j_2)}, c_{i_2+1}, \ldots, c_N;\boldsymbol{x}), \tag{29}$$

where $y_{i_1 i_2}(r_{i_1}^{(j_1)}, r_{i_2}^{(j_2)};\boldsymbol{x}) \equiv y(c_1, \ldots, c_{i_1-1}, r_{i_1}^{(j_1)}, c_{i_1+1}, \ldots, c_{i_2-1}, r_{i_2}^{(j_2)}, c_{i_2+1}, \ldots, c_N;\boldsymbol{x})$; $j_1, j_2 = 1, \ldots, n$. The procedure is repeated for all univariate and bivariate component functions, i.e., for all $y_i(r_i;\boldsymbol{x})$, $i = 1, \ldots, N$ and for all $y_{i_1 i_2}(r_{i_1}, r_{i_2};\boldsymbol{x})$, $i_1, i_2 = 1, \ldots, N$, leading to the univariate approximation

$$\hat{y}_1(\boldsymbol{R};\boldsymbol{x}) = \sum_{i=1}^{N} \sum_{j=1}^{n} \zeta_j(R_i) y(c_1, \ldots, c_{i-1}, r_i^{(j)}, c_{i+1}, \ldots, c_N;\boldsymbol{x}) - (N-1)y(\boldsymbol{c};\boldsymbol{x}) \tag{30}$$

and to the bivariate approximation

$$\hat{y}_2(\boldsymbol{R};\boldsymbol{x}) \equiv \sum_{\substack{i_1,i_2=1\\ i_1<i_2}}^{N}\sum_{j_2=1}^{n}\sum_{j_1=1}^{n}\zeta_{j_1}(R_{i_1})\zeta_{j_2}(R_{i_2})y(c_1,\ldots,c_{i_1-1},r_{i_1}^{(j_1)},c_{i_1+1},\ldots,c_{i_2-1},r_{i_2}^{(j_2)},c_{i_2+1},\ldots,c_N;\boldsymbol{x}) - (N-2)\sum_{i=1}^{N}\sum_{j=1}^{n}\zeta_j(R_i)y(c_1,\ldots,c_{i-1},r_i^{(j)},c_{i+1},\ldots,c_N;\boldsymbol{x}) + \frac{(N-1)(N-2)}{2}y(\boldsymbol{c};\boldsymbol{x}). \quad (31)$$

3.3. Monte Carlo simulation

Once the Lagrange shape functions $\zeta_j(r_i)$ and deterministic coefficients $y(\boldsymbol{c};\boldsymbol{x})$, $y(c_1,\ldots,c_{i-1},r_i^{(j)},c_{i+1},\ldots,c_N;\boldsymbol{x})$, and $y(c_1,\ldots,c_{i_1-1},r_{i_1}^{(j_1)},c_{i_1+1},\ldots,c_{i_2-1},r_{i_2}^{(j_2)},c_{i_2+1},\ldots,c_N;\boldsymbol{x})$ are generated, Eqs. (30) and (31) provide explicit approximations of an effective elastic property in terms of random input $\boldsymbol{R}$. Therefore, any probabilistic characteristics of the effective property, including its statistical moments and probability density function, can be easily evaluated by performing Monte Carlo simulation on Eqs. (30) and (31). For example, the lth moment of an effective elastic property $y(\boldsymbol{R};\boldsymbol{x})$ at a point $\boldsymbol{x}\in\mathscr{D}$ is

$$\mathbb{E}[y^l(\boldsymbol{R};\boldsymbol{x})] = \lim_{N_S\to\infty}\left[\frac{1}{N_S}\sum_{m=1}^{N_S}\hat{y}_S^l(\boldsymbol{r}_m;\boldsymbol{x})\right]; \quad l=1,2,\ldots,\infty, \quad (32)$$

where $\boldsymbol{r}_m$ is the mth sample of $\boldsymbol{R}$, $\hat{y}_S(\boldsymbol{r}_m;\boldsymbol{x})$ is the S-variate approximation of $y(\boldsymbol{r}_m;\boldsymbol{x})$, and N_S is the sample size. By setting $l=1$ and 2, and $S=1$ or 2 in Eq. (32), the univariate ($S=1$) or bivariate ($S=2$) approximations of the mean and standard deviation of an effective property can be obtained. The probability density function of an effective property can also be determined in a similar manner, e.g., by developing histograms from the generated samples. Since Eqs. (30) and (31) do not require solving additional micromechanical equations, the embedded Monte Carlo simulation can be efficiently conducted for any sample size. Note that $y(\boldsymbol{R};\boldsymbol{x})$ is a non-homogeneous output random field and hence, both the moments and probability density function of $y(\boldsymbol{R};\boldsymbol{x})$ depend on $\boldsymbol{x}\in\mathscr{D}$.

The stochastic methods involving univariate (Eq. (30)) or bivariate (Eq. (31)) approximations, n-point Lagrange interpolation (Eq. (28) or (29)), and associated Monte Carlo simulation are defined as the *univariate* or *bivariate decomposition method* in this paper.

3.4. Computational effort

The univariate and bivariate approximations require numerical function evaluations of $y(\boldsymbol{r};\boldsymbol{x})$ (e.g., solving micromechanical equations) to determine coefficients $y(\boldsymbol{c};\boldsymbol{x})$, $y(c_1,\ldots,c_{i-1},r_i^{(j)},c_{i+1},\ldots,c_N;\boldsymbol{x})$, and $y(c_1,\ldots,c_{i_1-1},r_{i_1}^{(j_1)},c_{i_1+1},\ldots,c_{i_2-1},r_{i_2}^{(j_2)},c_{i_2+1},\ldots,c_N;\boldsymbol{x})$ for $i,i_1,i_2=1,\ldots,N$ and $j,j_1,j_2=1,\ldots,n$. Hence, the computational effort required by the proposed method can be viewed as numerically solving a micromechanics problem at several deterministic input defined by user-selected sample points of $\boldsymbol{R}$. There are n and n^2 numerical evaluations of $y(\boldsymbol{r};\boldsymbol{x})$ involved in Eqs. (28) and (29), respectively. Therefore, the total cost for the univariate decomposition method entails a *maximum* of $nN+1$ function evaluations, and for the bivariate approximation, $N(N-1)n^2/2+nN+1$ *maximum* function evaluations are required. If the selected sample points include a common sample point in each coordinate r_i, the number of function evaluations reduces to $(n-1)N+1$ and $N(N-1)\times(n-1)^2/2+(n-1)N+1$ for univariate and bivariate methods, respectively.

The stochastic framework presented here in conjunction with the Mori–Tanaka model is not limited to a specific micromechanical formulation. For problems requiring more advanced deterministic formulations entailing finite element or other numerical analyses can be easily incorporated by replacing Eqs. (15)–(23) with their relevant equations or algorithms. In other words, any output function $y(\boldsymbol{R};\boldsymbol{x})$ associated with a selected deterministic micromechanical formulation is applicable for subsequent stochastic analysis. However, all numerical results reported in this paper are based on the Mori–Tanaka model.

4. Numerical examples

Four FGM examples including a limited effort of deterministic experimental validation are presented to illustrate various aspects of the stochastic micromechanical model developed. The material composition in Examples 1, 3, and 4 varies along a single dimension (x), leading to spatially-variant volume fractions $\phi_i(x)$; $i=1,2,3$. Since $\phi_1(x)+\phi_2(x)+\phi_3(x)=1$, only two volume fractions must be specified, such as the material volume fraction $\phi_2(x)$ of

phase 2 and the porosity volume fraction $\phi_3(x)$ of phase 3. In all examples, $\phi_i(x)$ is a one-dimensional Beta random field, which has the marginal probability density function (Ferrante and Graham-Brady, 2005)

$$f_i(\phi_i) = \begin{cases} \frac{1}{B(q_i,t_i)}\phi_i^{q_i-1}(1-\phi_i)^{t_i-1}, & 0 \leqslant \phi_i \leqslant 1 \\ 0, & \text{otherwise} \end{cases}, \tag{33}$$

where q_i and t_i are distribution parameters, $B(q_i,t_i) = \Gamma(q_i)\Gamma(t_i)/\Gamma(q_i+t_i)$ is the beta function, and $\Gamma(\tau) \equiv \int_0^\infty \exp(-\eta)\eta^{\tau-1}\,d\eta$ is the Gamma function. It has mean $\mu_i(x) = \sum_{j=0}^5 a_{i,j}x^j$ and standard deviation $\sigma_i(x) = \sum_{j=0}^5 b_{i,j}x^j$, where $a_{i,j}$ and $b_{i,j}$ are polynomial coefficients. The standardized volume fraction $\tilde{\phi}_i(x) \equiv [\phi_i(x) - \mu_i(x)]/\sigma_i(x)$, which has zero mean and unit variance, is also a Beta random field with its marginal probability distribution obtained from the prescribed Beta distribution of $\phi_i(x)$. In Examples 1, 3, and 4, the covariance function of $\tilde{\phi}_i(x)$ is $\Gamma_{\tilde{\phi}_i}(s) \equiv \mathbb{E}[\tilde{\phi}_i(x)\tilde{\phi}_i(x+s)] = \exp(-c_i|s|)$, where c_i is the correlation distance parameter. The transition region in Examples 3 and 4 is defined by $0.4 \leqslant \phi_2(x) \leqslant 0.6$.

In Examples 3 and 4, the univariate or bivariate decomposition method employed to calculate probabilistic characteristics of effective properties was formulated in the Gaussian image ($\boldsymbol{u}$ space) of the original space ($\boldsymbol{r}$ space) of the random input $\boldsymbol{R}$. The reference point $\boldsymbol{c} = 0$ and $n = 3$ was selected. In the $\boldsymbol{u}$ space, sample points $(c_1,\ldots,c_{i-1},u_i^{(j)},c_{i+1},\ldots,c_N)$ and $(c_1,\ldots,c_{i_1-1},u_{i_1}^{(j_1)},c_{i_1+1},\ldots,c_{i_2-1},u_{i_2}^{(j_2)},c_{i_2+1},\ldots,c_N)$ were chosen with $c_i = 0$ and uniformly distributed points $u_i^{(j)}$ or $u_{i_1}^{(j_1)}$ or $u_{i_2}^{(j_2)} = -1,0,1$. Therefore, $(n-1)N+1$ and $(n-1)^2N(N-1)/2+(n-1)N+1$ function evaluations are involved in univariate and bivariate methods, respectively.

4.1. Example 1

The first example entails evaluation of the adequacy of the K–L approximation for representing random phase volume fractions in three types of FGM. In type 1, a two-phase cenosphere-polyester FGM, prepared by dispersing aluminum silicate cenospheres (phase 2) in a polyester resin matrix (phase 1) (Parameswaran and Shukla, 2000), was examined. A three-phase Ni–MgO FGM comprising Ni (phase 1), MgO (phase 2), and porosity (phase 3) and another three-phase Ni_3Al–TiC FGM comprising Ni_3Al (phase 1), TiC (phase 2), and porosity (phase 3) define the remaining two FGM types (Zhai et al., 1993). In each FGM, the particle or porosity volume fraction varies along a single coordinate $0 \leqslant x \leqslant t$, where t denotes the total length of the variation. Measured volume fractions of cenosphere (i.e., $\phi_2(x)$ in type 1) and porosity (i.e., $\phi_3(x)$ in types 2 and 3) reported by Parameswaran and Shukla (2000) and Zhai et al. (1993) were employed to characterize $\mu_i(x)$, $\sigma_i(x)$, and $\Gamma_{\tilde{\phi}_i}(s)$. The parameters of these input functions are listed in Table 1. These second-moment properties, along with the assumption of Beta marginal distribution, completely describe the statistical characteristics of random volume fractions. In all three FGM types, the number of terms retained in the K–L approximation of the volume fraction was $M = 16$.

For $0 < \Gamma_{\tilde{\phi}_i} < 1$, Eq. (8) was solved to determine the required covariance function $\Gamma_{\alpha_i}(s)$. The $\Gamma_{\alpha_i} - \Gamma_{\tilde{\phi}_i}$ plot, depicted in Fig. 4, suggests that Γ_{α_i} is, indeed, very close to $\Gamma_{\tilde{\phi}_i}$. Therefore, $\Gamma_{\alpha_i}(s)$ can also be satisfactorily approximated by the exponential covariance kernel. The eigensolutions of $\Gamma_{\alpha_i}(s)$ were obtained analytically (Ghanem and Spanos, 1991).

Fig. 5(a) presents experimentally measured scatter plots of the cenosphere volume fraction as a function of the normalized spatial coordinate (x/t). The scatter is due to sample-to-sample variability observed in various specimens of the

Table 1
Second-moment characteristics of volume fractions in three FGMs

Parameters	Cenosphere polyester ($i=2$)[a]	Ni–MgO ($i=3$)[b]	Ni_3Al–TiC ($i=3$)[b]
$a_{i,0}$	0	0.069	0.034
$a_{i,1}$	0.109	0.85	0.087
$a_{i,2}$	4.25	−3.67	−0.936
$a_{i,3}$	−9.762	12.866	2.831
$a_{i,4}$	8.629	−17.181	−3.543
$a_{i,5}$	−2.748	7.356	1.618
$b_{i,0}$	0	0.012	0.001
$b_{i,1}$	0.178	0.118	0.014
$b_{i,2}$	−0.309	−0.976	−0.078
$b_{i,3}$	0.155	3.461	0.156
$b_{i,4}$	0	−4.798	−0.14
$b_{i,5}$	0	2.205	0.049
c_i	5	5	5

[a] For particle: $\mu_2(x) = \sum_{j=0}^5 a_{2,j}x^j$; $\sigma_2(x) = \sum_{j=0}^5 b_{2,j}x^j$; $\Gamma_{\tilde{\phi}_2}(s) = \exp(-c_2|s|)$.

[b] For porosity: $\mu_3(x) = \sum_{j=0}^5 a_{3,j}x^j$; $\sigma_3(x) = \sum_{j=0}^5 b_{3,j}x^j$; $\Gamma_{\tilde{\phi}_3}(s) = \exp(-c_3|s|)$.

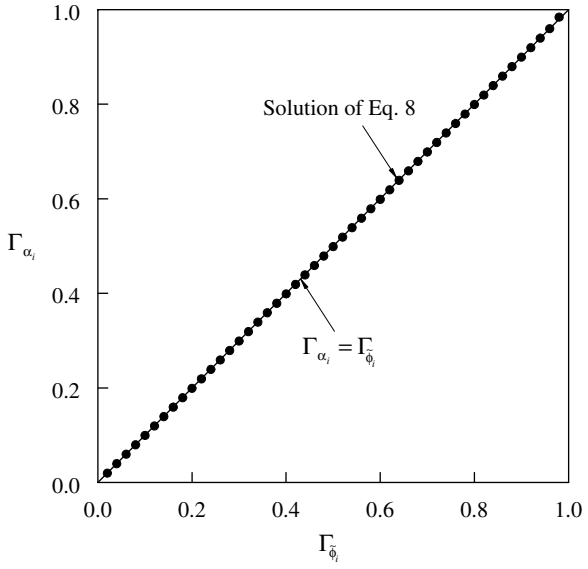

Fig. 4. Covariance functions Γ_{α_i} vs. $\Gamma_{\tilde{\phi}_i}$.

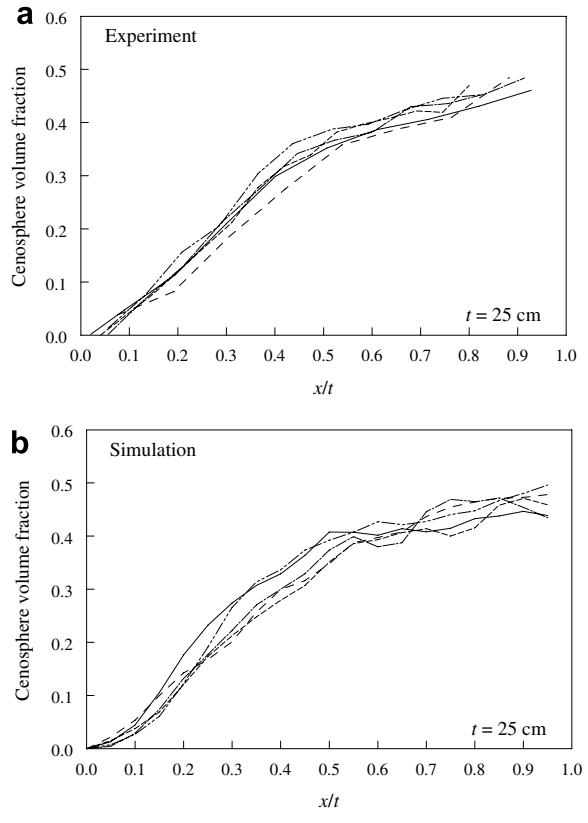

Fig. 5. Cenosphere volume fraction: (a) experiment; (b) simulation.

cenosphere-polyester FGM (Parameswaran and Shukla, 2000). By generating realizations of standard Gaussian random variables $Z_{i,k}$; $i = 2$; $k = 1, \ldots, 16$ and invoking Eqs. (5) and (14), samples of the cenosphere volume fraction were determined. The predicted (simulated) samples of the cenosphere volume fraction, presented in Fig. 5(b), are in close agreement with experimental samples in Fig. 5(a). The second-moment properties of the simulated volume fraction were obtained from the experimental data.

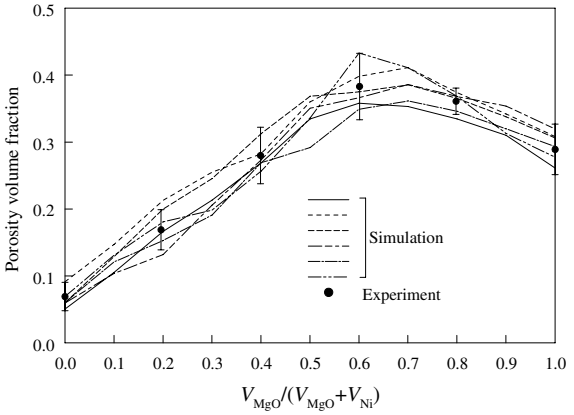

Fig. 6. Porosity volume fraction in Ni–MgO FGM.

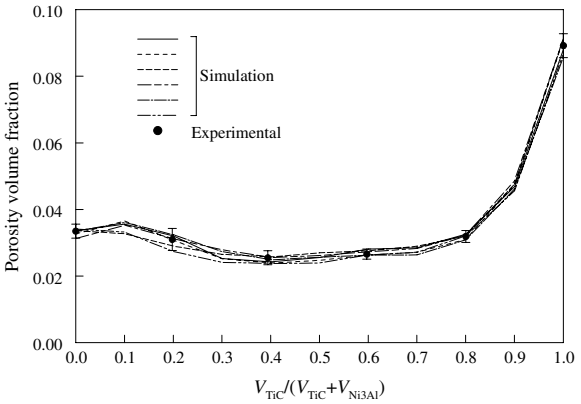

Fig. 7. Porosity volume fraction in Ni_3Al–TiC FGM.

Figs. 6 and 7 show simulated samples of random volume fractions of porosity in the Ni–MgO FGM and the Ni_3Al–TiC FGM, which are plotted against relative volume fractions $V_{MgO}/(V_{MgO} + V_{Ni})$ and $V_{TiC}/(V_{TiC} + V_{Ni_3Al})$, respectively, where V indicates volume and its subscripts denote material phases. The predicted samples from the proposed random field model with calibrated second-moment properties and assuming Beta marginal distribution compare well with experimental data (Zhai et al., 1993) available at selected points. Both experimen-

tal data and simulated samples indicate larger porosity and larger scatter of porosity in Ni–MgO FGM than in Ni_3Al–TiC FGM. Figs. 5–7 demonstrate the usefulness of the proposed random field model in accurately simulating spatial variability of phase volume fractions.

4.2. Example 2

The objective of Example 2 is to deterministically validate the three-phase Mori–Tanaka model, i.e., Eqs. (15)–(22) in predicting effective properties of heterogeneous materials. The validation effort is focused on evaluating effective elastic modulus ($\overline{E}$) of three types of composites in which the particle and/or porosity are uniformly distributed (Cohen and Ishai, 1967): (1) *porous matrix*, where porosity in the epoxy matrix (50% shell epicote 815 and 50% versamid 140 by weight) ranges from 1.7% to 34%; (2) *non-porous composite*, where silica (Ottawa sand) particles in the epoxy matrix have volume fractions varying from 8% to 27.75%; and (3) *porous composite*, where both silica particles and porosity co-exist and have respective volume fractions varying from 12% to 33.25% and 10% to 30.5%. The elastic properties of constituents are: $E_m = 22{,}000\ \text{kg/cm}^2$; $E_p = 750{,}000\ \text{kg/cm}^2$; $v_m = 0.3$; and $v_p = 0.25$, where the subscripts m and p indicate matrix and particle, respectively (Cohen and Ishai, 1967). No statistical uncertainties were included in this example. The micromechanical analysis of the porous matrix was conducted by forcing $\phi_p(x) = \phi_v(x)$ and using degenerative properties of voids. For the non-porous composite, $\phi_v(x) = 0$.

Table 2
Predicted and experimental elastic moduli of porous matrix

Porosity volume fraction, %	$\overline{E}/E_m$ [a]	
	Predicted	Experimental (Cohen and Ishai, 1967)
1.7	0.97	0.97
7.9	0.85	0.79
9	0.83	0.82
13.5	0.76	0.72
15	0.73	0.69
16.75	0.71	0.68
18.2	0.69	0.64
20.9	0.65	0.62
26	0.58	0.57
28	0.56	0.55
32	0.51	0.48
34	0.49	0.45

[a] $\overline{E}$ = effective elastic modulus; E_m = elastic modulus of matrix.

Table 3
Predicted and experimental elastic moduli of non-porous composite

Particle volume fraction, %	$\overline{E}/E_m$ [a]	
	Predicted	Experimental (Cohen and Ishai, 1967)
8	1.22	1.15
12	1.32	1.21
15.75	1.42	1.4
18.25	1.49	1.52
22.25	1.61	1.68
23.25	1.65	1.73
23.5	1.66	1.74
26.25	1.75	1.86
26.75	1.76	1.89
27.75	1.8	2

[a] $\overline{E}$ = effective elastic modulus; E_m = elastic modulus of matrix.

Table 4
Predicted and experimental elastic moduli of porous composite

Particle volume fraction, %	Porosity volume fraction, %	$\overline{E}/E_m$ [a]	
		Predicted	Experimental (Cohen and Ishai, 1967)
12	30.5	0.68	0.66
15.75	10	1.11	1.15
18.25	38	0.65	0.57
22.25	25	0.97	1.13
23.25	21.5	1.06	1.07
23.5	20	1.1	1.17
26.25	31.25	0.87	0.81
26.75	10	1.43	1.73
27.75	6.5	1.57	1.9
33.25	14	1.49	1.48

[a] $\overline{E}$ = effective elastic modulus; E_m = elastic modulus of matrix.

Tables 2–4 respectively list predicted values of the normalized effective modulus $\overline{E}/E_m$ for porous matrix, non-porous composite, and porous composite, calculated for various input values of porosity and/or particle volume fractions. Compared with experimental measurements of $\overline{E}/E_m$, also presented in Tables 2–4, the Mori–Tanaka model provides reasonably accurate estimates of the effective properties of heterogeneous materials considered in this study. The average errors in the prediction relative to experimental results are 4.7%, 5.5%, and 8.5% for porous matrix, non-porous composite, and porous composite, respectively.

4.3. Example 3

Consider again three FGM types defined in Example 1. The two-phase cenosphere-polyester FGM (type 1) includes polyester and cenosphere as phases 1 and 2. The three-phase Ni–MgO FGM (type 2) includes Ni, MgO, and porosity; and the three-phase Ni_3Al–TiC FGM (type 3) includes Ni_3Al, TiC, and porosity as phases 1, 2, and 3. In addition to random field models of stochastic volume fractions of phase 2 (cenosphere) in type 1 and of stochastic volume fractions of phase 3 (porosity) in types 2 and 3, the elastic moduli E_1 and E_2 and Poisson's ratios ν_1 and ν_2 of constituent materials were assumed to be independent lognormal random variables. Means and coefficients of variation of these constituents for each FGM are defined in Table 5. Using $M = 16$ for the K–L approximations of $\tilde{\phi}_2(x)$ or $\tilde{\phi}_3(x)$, the total number of random variables is $N = M + 4 = 20$. The univariate decomposition method was employed to calculate second-moment characteristics of the effective properties of all three FGMs.

Fig. 8 depicts plots of both predicted mean and standard deviation of the effective elastic modulus of the cenosphere-polyester FGM for $0 \leqslant x/t \leqslant 1$. The high-low experimental data of Parameswaran and Shukla (2000), plotted in Fig. 8, indicate good agreement between experimental and predicted means when $x/t \leqslant 0.75$. However, the predicted mean at $x/t = 0.86$ is much lower than its experimental value. The underprediction did not improve when using the results of an alternative micromechanical model that includes particle interactions (Yin et al., 2004), also plotted in Fig. 8. It is not clear why the experimental modulus at $x/t = 0.86$ is larger than both micromechanical predictions.

Table 5
Statistical properties of constituents in three FGMs[a]

Random variable	Mean	Coefficient of variation, %
Cenosphere-polyester[b]		
E_1 (GPa)	3.6	0.1
E_2 (GPa)	6	0.15
ν_1	0.41	0.1
ν_2	0.35	0.15
Ni–MgO[c]		
E_1 (GPa)	146	0.1
E_2 (GPa)	104	0.1
ν_1	0.35	0.1
ν_2	0.16	0.1
Ni_3Al–TiC[d]		
E_1 (GPa)	199	0.15
E_2 (GPa)	460	0.15
ν_1	0.295	0.15
ν_2	0.19	0.15

[a] Random variables are independent and lognormal.
[b] 1 = polyester; 2 = cenosphere.
[c] 1 = Ni; 2 = MgO.
[d] 1 = Ni_3Al; 2 = TiC.

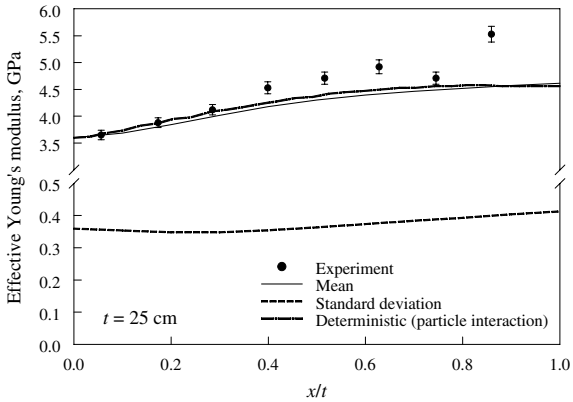

Fig. 8. Mean and standard deviation of effective modulus of cenosphere-polyester FGM.

Fig. 9(a) and (b) present second-moment characteristics of effective modulus and effective Poisson's ratio, respectively, of the Ni–MgO FGM, obtained by the proposed stochastic model. The statistics are plotted against the relative volume fraction $V_{MgO}/(V_{MgO} + V_{Ni})$. The predicted mean curves correlate well with the experimental trend. Deterministic results from two alternative models based on the mean-field theory (Zhai et al., 1993) and VCFEM (Grujicic and Zhang, 1998), plotted in Fig. 9(a) and (b), also indicate their satisfactory performance. The predicted means employing the Mori–Tanaka model and deterministic results by the mean-field theory (Zhai et al., 1993), the particle interaction model (Yin et al., 2004) and VCFEM (Grujicic and Zhang, 1998) for the Ni_3Al–TiC FGM, presented in Fig. 10(a) and (b) for effective elastic modulus and Poisson's ratio, respectively, also compare fairly well with the associated experimental data.

In addition to the mean response, the decomposition method provides standard deviations of the effective properties of both Ni–MgO and Ni_3Al–TiC FGMs, calculated without (option 1) and with (option 2) variability of constituent material properties, as shown in Figs. 9 and 10. Due to the small randomness of the porosity volume fraction of Ni_3Al–TiC FGM (Fig. 7), the standard deviations of the effective properties calculated without constit-

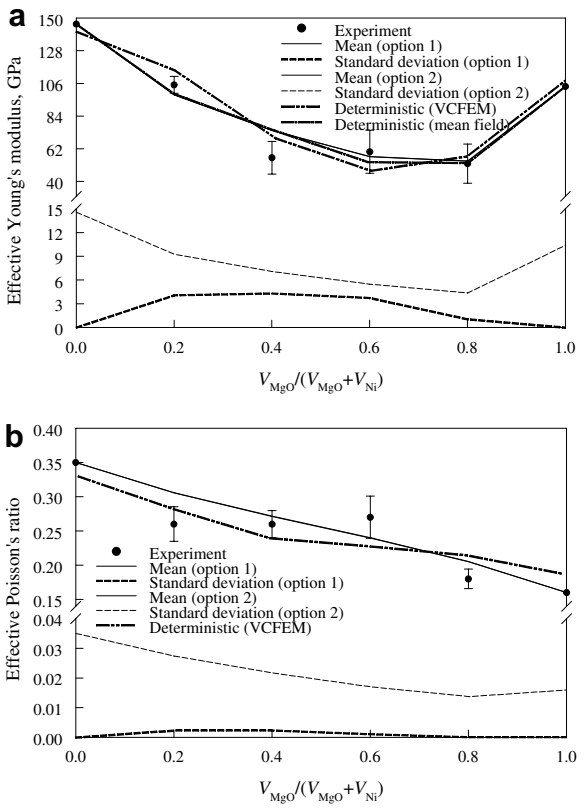

Fig. 9. Mean and standard deviation of effective properties of Ni–MgO FGM: (a) elastic modulus; (b) Poisson's ratio.

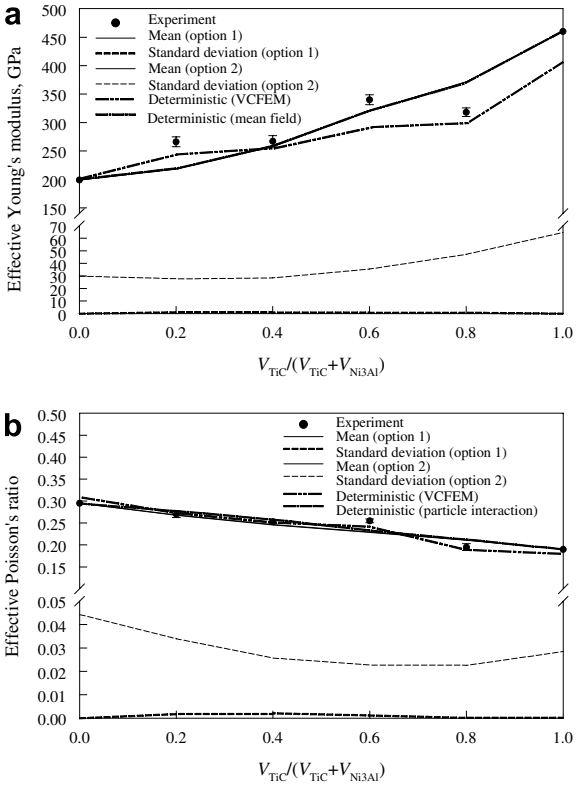

Fig. 10. Mean and standard deviation of effective properties of Ni_3Al–TiC FGM: (a) elastic modulus; (b) Poisson's ratio.

uent material property variations in Fig. 10(a) and (b) are also small and hence negligible. However, the standard deviations of the effective elastic modulus of the Ni–MgO FGM in Fig. 9(a), which entails large randomness of the porosity volume fraction (Fig. 6), are dependent on variations of both the constituent material property and porosity volume fraction. In both FGMs, the randomness of the porosity volume fraction has a negligible effect on the variability of the Poisson's ratio.

4.4. Example 4

The final example entails evaluating probability density functions of effective FGM properties by propagating input uncertainties via the stochastic micromechanical model developed. Consider again an FGM system with the material composition varying along a single coordinate $0 \leqslant x \leqslant t$, where t denotes the total length of the variation. Means and coefficients of variation of constituent elastic properties, which follow independent lognormal distribution, are defined in Table 6. The particle (phase 2) and porosity (phase 3) volume fractions $\phi_2(x)$ and $\phi_3(x)$ were modeled as non-homogeneous, Beta random fields with respective means $\mu_2(x) = \bar{x}$ and $\mu_3(x) = 0.1\bar{x}(1-\bar{x})$, respective standard deviations $\sigma_2(x) = 0.6\bar{x}(1-\bar{x})$ and $\sigma_3(x) = 0.1\bar{x}(1-\bar{x})$, where $\bar{x} = x/t$ and covariance functions $\Gamma_{\tilde{\phi}_2}(s) = \Gamma_{\tilde{\phi}_2}(s) = \exp(-5|s|)$. The Gaussian image field $\alpha_i(x)$ of $\tilde{\phi}_i(x)$ was parameterized using 8 random variables. Therefore, the input random vector is $\boldsymbol{R} = \{Z_{2,1}, \ldots, Z_{2,8}, Z_{3,1}, \ldots, Z_{3,8}, E_1, E_2, \nu_1, \nu_2\}^{\mathrm{T}} \in \mathbb{R}^N$, where the total number of random variables is $N = 2 \times 8 + 4 = 20$.

Table 6
Statistical properties of constituents in an FGM[a]

Random variable	Mean	Coefficient of variation (%)
E_1 (GPa)	199	0.1
E_2 (GPa)	460	0.15
ν_1	0.295	0.1
ν_2	0.19	0.15

[a] Random variables are independent and lognormal.

Fig. 11(a) and (b) compare predicted probability densities and/or histograms of the effective elastic

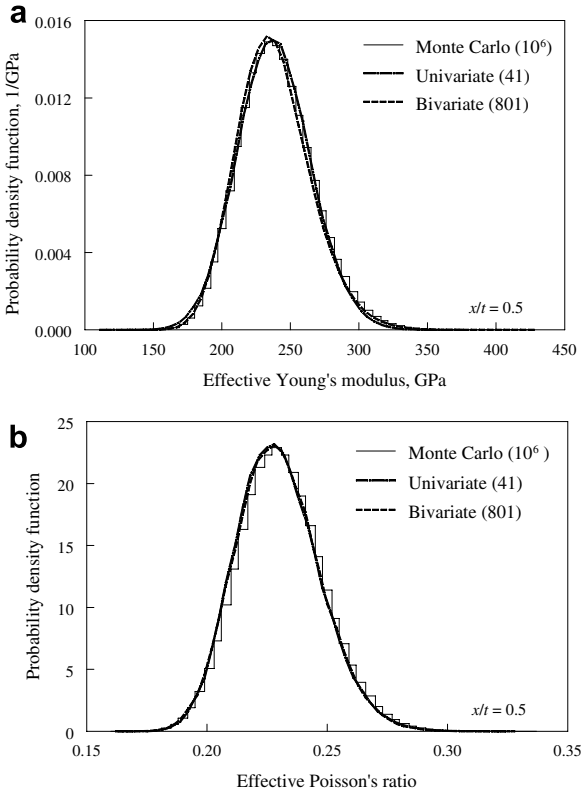

Fig. 11. Probability densities of FGM effective properties at $x/t = 0.5$ by various methods: (a) elastic modulus; (b) Poisson's ratio.

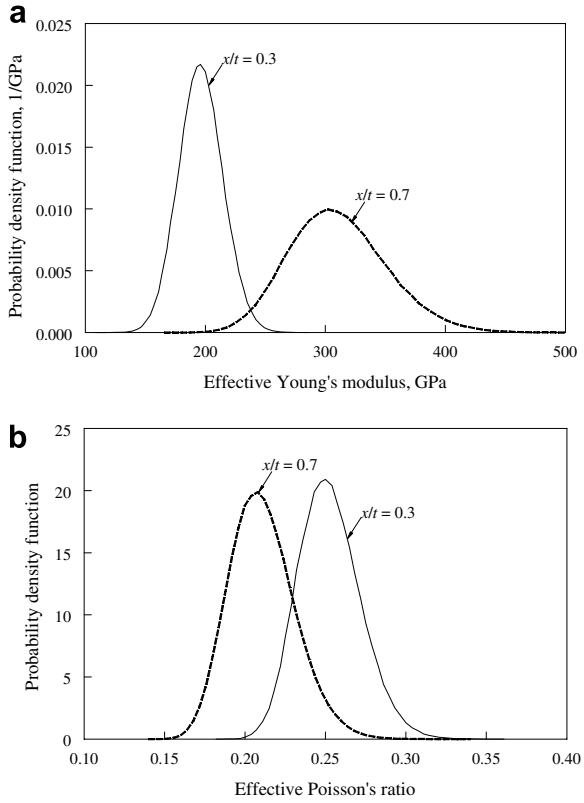

Fig. 12. Probability densities of FGM effective properties by the univariate method at two different locations: (a) elastic modulus; (b) Poisson's ratio.

modulus and Poisson's ratio at $x/t = 0.5$ by the univariate and bivariate decomposition methods and the direct Monte Carlo simulation involving 10^6 samples. The decomposition method, which entails Monte Carlo analysis employing the univariate or bivariate approximations in Eqs. (11) or (12), permits inexpensive calculation of the effective modulus by sidestepping additional micromechanical analyses. Compared with the direct Monte Carlo simulation, the univariate method retaining only individual effects of random variables yields a very accurate estimate of the probability densities of the effective properties. The bivariate method, which includes both individual and cooperative effects of random variables, also provides excellent results. No meaningful difference in the results of univariate and bivariate methods was observed in this particular example. Therefore, the univariate method can be employed for subsequent calculations. Using $n = 3$ and $N = 20$, the univariate and bivariate decomposition methods involve only 41 and 801 function evaluations (micromechanical analyses), respectively, whereas 10^6 analyses were performed by the direct Monte Carlo simulation. Therefore, the decomposition method developed, in particular the univariate version, is not only accurate, but also computationally efficient.

Using the univariate decomposition method, the probability densities of the effective elastic modulus at $x/t = 0.3$ and 0.7 are presented in Fig. 12(a); and the probability densities of the Poisson's ratio at $x/t = 0.3$ and 0.7 are presented in Fig. 12(b). These probability densities, which can be evaluated at any spatial location, should provide useful information for reliability analysis and reliability-based design optimization of FGMs.

5. Conclusions

A stochastic micromechanical model was developed for predicting probabilistic characteristics of elastic mechanical properties of an isotropic functionally graded material (FGM) subject to statistical uncertainties in material properties of constituents

and their respective volume fractions. The model involves: (1) non-homogeneous, non-Gaussian random field representation of phase volume fractions and random variable description of constituent material properties; (2) a three-phase Mori–Tanaka model for underlying micromechanics and homogenization; and (3) a novel dimensional decomposition method for obtaining statistical moments and probabilistic density functions of effective FGM properties. The proposed decomposition results in a finite, hierarchical, and convergent series for an effective elastic property of interest. The computational effort in finding probabilistic characteristics of an effective property can be viewed as performing deterministic micromechanical analyses at selected input defined by sample points. Hence, alternative micromechanical formulations can be easily embedded in the proposed stochastic model. Results of numerical examples indicate that the stochastic model developed provides accurate representation of spatial variability in phase volume fractions and yields accurate probabilistic characteristics of effective elastic properties of FGM. The underlying deterministic analysis employing a three-phase Mori–Tanaka model also provides excellent prediction of effective properties of several heterogeneous media examined in this work. The computational efforts required by the univariate and bivariate versions of the decomposition method are linear and quadratic with respect to the number of random variables involved. Therefore, the model developed is also computationally efficient when compared with the direct Monte Carlo simulation.

Acknowledgements

The authors would like to acknowledge financial support of the US National Science Foundation under Grant No. CMS-0409463.

References

Aboudi, J., Pindera, M.J., Arnold, S.M., 1996. Thermoelastic theory for the response of materials functionally graded in two directions. International Journal of Solids and Structures 33, 931–966.

Buryachenko, V.A., Rammerstorfer, F.G., 2001. Local effective thermoelastic properties of graded random structure matrix composites. Archive of Applied Mechanics 71, 249–272.

Cohen, L.J., Ishai, O., 1967. The elastic properties of three-phase composites. Journal of Composite Materials 1, 390–403.

Davenport, W.B., Root, W.L., 1958. An Introduction to the Theory of Random Signals and Noise. McGraw-Hill, New York.

Eshelby, J.D., 1957. The determination of the elastic field of an ellipsoidal inclusion and related problems. Proceedings of the Royal Society of London; Series A 241, 376–396.

Ferrante, F.J., Graham-Brady, L.L., 2005. Stochastic simulation of non-gaussian/non-stationary properties in a functionally graded plate. Computer Methods in Applied Mechanics and Engineering 194, 1675–1692.

Ghanem, P.D., Spanos, P.D., 1991. Stochastic Finite Elements: A Spectral Approach. Springer-Verlag, New York, NY.

Grigoriu, M., 1995. Applied Non-Gaussian Processes: Examples, Theory, Simulation, Linear Random Vibration, and MATLAB Solutions. Prentice-Hall, Englewood Cliffs, NJ.

Grujicic, M., Zhang, Y., 1998. Determination of effective elastic properties of functionally graded materials using Voronoi cell finite element method. Materials Science and Engineering A 251, 64–76.

Hashin, Z., Strikman, S., 1963. A variational approach to the theory of the elastic behavior of multi-phase materials. Journal of the Mechanics and Physics of Solids 11, 127–140.

Hill, R., 1965. A self-consistent mechanics of composite materials. Journal of the Mechanics and Physics of Solids 13, 213–222.

Mori, T., Tanaka, K., 1973. Average stress in matrix and average elastic energy of material with misfitting inclusions. Acta Materialia 21, 571–574.

Mura, T., 1991. Micromechanics of Defects in Solids, second revised ed. Kluwer Academic Publishers, Dordrecht, The Netherlands.

Nemat-Nasser, S., Hori, M., 1999. Micromechanics: Overall Properties of Heterogeneous Materials, second ed. North-Holland, Amsterdam, The Netherlands.

Parameswaran, V., Shukla, A., 2000. Processing and characterization of a model functionally gradient material. Journal of Material Science 35, 21–29.

Rahman, S., Xu, H., 2005. A meshless method for computational stochastic mechanics. International Journal of Computational Methods in Engineering Science and Mechanics 64, 41–58.

Suresh, S., 2001. Graded materials for resistance to contact deformation and damage. Science 292, 2447–2451.

Suresh, S., Mortensen, A., 1998. Fundamentals of Functionally Graded Materials. Institute of Materials, London.

Weng, G.J., 1984. Some elastic properties of reinforced solids, with special reference to isotropic ones containing spherical inclusions. International Journal of Engineering Science 22 (7), 845–856.

Xu, H., Rahman, S., 2004. A generalized dimension-reduction method for multi-dimensional integration in stochastic mechanics. International Journal for Numerical Methods in Engineering 61, 1992–2019.

Xu, H., Rahman, S., 2005. Decomposition methods for structural reliability analysis. Probabilistic Engineering Mechanics 20, 239–250.

Yin, H.M., Sun, L.Z., Paulino, G.H., 2004. Micromechanics-based elastic model for functionally graded materials with particle interactions. Acta Materialia 52, 3535–3543.

Zhai, P.C., Jiang, C.R., Zhang, Q.J., 1993. Application of three-phase micromechanical theories to ceramic/metal functionally gradient materials. In: Holt, J.B., Koizumi, M., Hirari, T., Munir, Z. (Eds.), Ceramic Transactions: Functionally Gradient Materials. The American Ceramic Society, Westerville, OH, pp. 449–456.